UNSTEADY CRITERIA FOR ROTOR BLADE AIRFOIL DESIGN

A. Klein[1], K. Richter[2], A. Altmikus[3], Th. Lutz[1], E. Krämer[1]

[1]Institute of Aerodynamics and Gas Dynamics
Universität Stuttgart
Pfaffenwaldring 21, 70569 Stuttgart, Germany

[2]Institute of Aerodynamics and Flow Technology
German Aerospace Center (DLR)
Bunsenstraße 10, 37073 Göttingen, Germany

[3]Eurocopter Deutschland GmbH
81663 München, Germany

Abstract

The present paper deals with the definition and application of different unsteady criteria that may be considered in a dedicated aerodynamic design of rotorcraft airfoils. Today's airfoil design methodologies for rotorcraft applications rely on steady computations and design criteria. Due to the inherent flow unsteadiness at forward flight, caused by variable incoming flow velocity, cyclic pitching as well as blade motion and deformation, it is however deemed necessary to further take into account unsteady aerodynamic effects and characteristics of the airfoil in the design process. Unsteady criteria are introduced for both 2D rotor-environment simulations with varying free-stream Mach number and angle of attack and for high-frequency, small amplitude harmonic pitch oscillations at constant Mach number. By means of URANS simulations, with numerical settings validated against experiments, these criteria are exemplarily applied to the OA209 rotor blade airfoil geometry.

NOMENCLATURE

Symbols

b	airfoil model span
c	airfoil chord length
C_d	drag coefficient
C_l	lift coefficient
C_m	pitching moment coefficient
f	frequency
k	reduced frequency, $k = \pi f c / U_\infty$
M	Mach number
p	pressure
r/R	radius position of airfoil
R	rotor radius
Re	Reynolds number based on chord length
S	aerodynamic damping
S^*	damping coefficient
U_∞	free-stream velocity
v	forward flight speed
y^+	dimensionless wall distance
α	incidence angle
$\Delta\alpha$	pitching amplitude
Ψ	blade azimuth angle
ω	angular velocity

Subscripts

ref	based on common reference
sh	shock induced
max	maximum value

Acronyms

CFD	Computational Fluid Dynamics
DFT	Discrete Fourier Transform
GOAHEAD	Generation of Advanced Helicopter Experimental Aerodynamic Database
HOST	Helicopter Overall Simulation Tool
TWG	Transonic wind tunnel Göttingen

1. INTRODUCTION

Performance and trim calculations of helicopter rotors nowadays are largely based on blade element momentum theory, whereby the blade section aerodynamics stem from numerically or experimentally gained steady polars. The different requirements and flow conditions within the rotor environment are taken into account in two-dimensional airfoil design only by multi-objective steady design criteria. Unsteady aerodynamic effects such as hystereses of the aerodynamic coefficients and dynamic stall, cannot be accounted for in this approach. However, since unsteady phenomena can be a source of large dynamic loads, aerodynamic airfoil design should aim at providing geometries that are good-natured in this respect, and therefore requires a means of unsteady airfoil assessment.

The objective of the present paper is to introduce the consideration of unsteady characteristics within the airfoil design process. Towards this goal, the present paper defines unsteady criteria for the evaluation of airfoil geometries. The criteria can be used to assess the effect of airfoil shape modifications on the unsteady behavior and derive correlations between geometric parameters, steady and unsteady characteristics.

2. UNSTEADY AIRFOIL CHARACTERISTICS

The blade section at a given radial position of the main rotor experiences a wide variety of flow conditions due to the combination of rotor speed, downwash and flight velocity of the helicopter. The cyclic pitching used for the redistribution of forces over the rotor disk introduces a large range of transient incidence angles combined with variations of incoming Mach number. Furthermore, elastic deformations (mainly torsion) as well as heaving and lagging motions of the rotor blade change the effective angle of attack for any blade section.

The most prominent unsteady aerodynamic features on the rotor include the dynamic stall phenomenon on the retreating blade and hysteresis loops of the aerodynamic coefficients. The hysteresis loop for harmonic pitching of an airfoil with attached flow at constant inflow velocity can be theoretically approximated by inviscid, incompressible Theodorsen's theory [1], and there exist a number of semi-empirical dynamic stall models of which the Leishman-Beddoes model and variants thereof [2,3] have been widely applied in the past. While these theories and models are able to roughly predict unsteady aerodynamic effects, they do not give the airfoil designer a tool at hand which would allow considering all rotor-relevant unsteady airfoil characteristics during design. Indeed, the complexity of the rotor environment violates some of the inherent assumptions of these models. Furthermore, there are several additional unsteady aspects of great importance with regard to performance, loads and stability.

2.1. Industrial aspects

As helicopter manufacturers strive for improved performance, reduced operational costs and longer maintenance intervals, the airfoil design comes back into the focus of the rotor designer as one of the numerous "parameters" he might be able to beneficially exploit. On the background of the availability of improved numerical methods and high computational power it seems feasible today to design new airfoils that feature improved performance characteristics while assuring benign unsteady characteristics.

Of course, performance is ever an important issue. And it is well known that retreating blade stall in high speed forward flight increases power required. Increasing the rotor speed to help the retreating side is limited by advancing blade drag. Active rotors that might offer a solution [4] are still far from serialisation. An advanced compromise airfoil design with controlled unsteady behaviour i.e. a delayed stall onset seems to be a good near-term option.

While realising performance gains by aerodynamic airfoil design, it is important to monitor the implications on control system loads and vibrations.

Controlling dynamic pitch link loads has particular importance when retrofit scenarios are discussed where the normal ambition is to realise rotor performance gains with as little changes to the dynamic system as possible.

The meaning of dynamic pitch link loads to fatigue of the control system components must be stressed, because fatigue relevant load cycles are quickly accumulated in specific highly loaded flight conditions. Subsequently, life cycle of parts may deteriorate quickly. Moreover, the pilot usually does not recognise these harmful load conditions, when an extraordinary pitching moment stall occurs.

Finally, unsteady aerodynamic excitation of the flexible blade structure leading to an increase in vibration in flight conditions near the stall boundary needs to be addressed.

2.2. Definition of unsteady criteria

The dynamic loads on the pitch control rods due to dynamic stall and torsional blade oscillations are one of the most urgent issues concerning unsteady effects. Therefore, the focus of the unsteady simulations and criteria is to assess the pitching moment stability of the airfoil. The torsional excitation of the first blade eigenmode observed in practice may be due to either

- aerodynamic excitation of the blade torsion in response to the 1/rev kinematic motion and the associated dynamic stall phenomenon that can show higher frequency content especially during the downstroke phase (vortex shedding)

or

- fluid-structure interaction at the blade eigenfrequency due to higher harmonic kinematics near 4-6/rev and undamped aerodynamic response in the same frequency range.

To investigate both of these scenarios, two different environments are defined for which the unsteady evaluation is performed. First, the blade kinematics and varying onflow conditions are taken into account in the main rotor environment. Secondly, high-frequency, small

amplitude harmonic pitch oscillations at medium to high angle of attack and constant Mach number are checked for negative aerodynamic damping.

2.2.1. Rotor environment

For the rotor environment calculations, the flow conditions at a given radial position are used to define the 2D onflow as seen by the local blade section during one rotor-cycle. This approach is valid for any trimmed state of the main rotor where periodic flow conditions are ensured. Fig. 1 presents an exemplary distribution of effective angle of attack and Mach number over azimuth angle for such a scenario. The corresponding angle of attack and Mach number Fourier coefficients are given by Tab. 1 and 2, respectively.
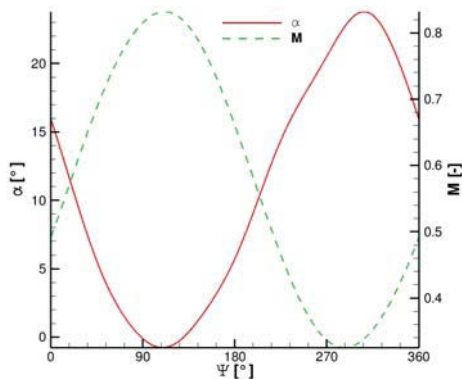
Figure 1: Distribution of effective angle of attack and Mach number at radial position r/R=0.954 during one rotor-cycle, GOAHEAD test case v=317 km/h

Fourier mode		0
alpha		10.7494
	1c	1s
alpha	5.0782	-10.8146
	2c	2s
alpha	0.3132	-0.9800
	3c	3s
alpha	-0.0553	-0.3694
	4c	4s
alpha	-0.2171	0.0029
	5c	5s
alpha	0.0802	0.1220
	6c	6s
alpha	-0.0020	0.0143

Table 1: Fourier coefficients of effective angle of attack, r/R=0.954, GOAHEAD test case v=317 km/h

Fourier mode		0
M		0.5773
	1c	1s
M	-0.0836	0.2399
	2c	2s
M	0.0002	-0.0024
	3c	3s
M	-0.0006	0.0003
	4c	4s
M	-0.0013	0.0002

Table 2: Fourier coefficients of local Mach number, r/R=0.954, GOAHEAD test case v=317 km/h

2.2.1.1. Performance

While the current 2D approach neglects 3D-effects on the rotor, such as crossflow, Coriolis forces and tip vortices, the averaged values of the aerodynamic coefficients over one rotor-cycle give a good estimate of the aerodynamic performance and loads of the blade section.

$$(1) \qquad \overline{C_l} = \frac{1}{2\pi} \int_0^{2\pi} C_{l,ref}(\Psi) d\Psi$$

$$(2) \qquad \overline{C_d} = \frac{1}{2\pi} \int_0^{2\pi} C_{d,ref}(\Psi) d\Psi$$

$$(3) \qquad \overline{C_m} = \frac{1}{2\pi} \int_0^{2\pi} C_{m,ref}(\Psi) d\Psi$$

The subscript 'ref' refers to a common constant reference Mach number or dynamic pressure which is used rather than the local dynamic pressure that varies with azimuth angle. Typically, for rotorcraft applications the rotor tip speed in hover is used as the reference value. The common reference is mandatory to define meaningful load averages which can be interpreted as thrust, power and mean pitching moment of an annulus at the given radial position of the airfoil.

2.2.1.2. Pitching moment and damping

The Liiva criterion has previously been defined as a measure of the moment stability [5] since negative aerodynamic damping is considered highly relevant for dynamic pitch link loads on the helicopter rotor. The damping factor S* is defined as the closed-loop integral S of the pitching moment, non-dimensionalized by the theoretical value S_{theory} derived from Theodorsen's theory:

$$(4) \qquad S* = \frac{S}{S_{theory}}$$

with

$$(5) \qquad S = -\oint_\alpha C_m d\alpha$$

$$(6) \qquad S_{theory} = \frac{\pi^2}{2} \cdot k \cdot \Delta\alpha^2 \geq 0$$

This criterion is only meaningful when analyzed for the forcing kinematic frequency. For purely sinusoidal pitching only the first harmonic of the moment coefficient will contribute to the moment integral and the damping coefficient. As variable freestream conditions and higher harmonic pitching violate some of the inherent assumptions of the Liiva criterion, it is proposed to analyze the aerodynamic damping independently for each oscillatory excitation frequency in case of rotor cycle calculations:

$$(7) \qquad S = -\oint_\alpha C_{m,ref} d\alpha$$

$$(8) \qquad S_i = -\oint_\alpha C_{m,ref,i/rev}\,d\alpha$$

Blade stability can be further examined through comparison of higher mode amplitudes of the pitching moment near the blade torsional eigenfrequencies. This analysis shall check for the aforementioned aerodynamic excitation of the blade torsion in response to the 1/rev kinematic motion and the associated dynamic stall phenomenon.

Finally, the peak-to-peak values of the pitching moment coefficient are evaluated, both for the first pitching moment stall $\Delta C_{m,sh}$ and for the highest C_m amplitude during the following vortex-shedding process, $\Delta C_{m,max}$ (see Fig. 7). The denotation $\Delta C_{m,sh}$ for the first moment stall event is chosen in the present investigation of fast forward flight, since in this case the drop in pitching moment is caused by upstream shock movement and the associated enlargement of boundary layer separation (see section 4.1). The two peak-to-peak values estimate the magnitude of the dynamic pitch-link loads experienced by the rotor.

2.2.2. High-frequency oscillations

Possible fluid-structure interaction at the blade torsional eigenfrequency due to higher harmonic pitch oscillations and undamped aerodynamic response is to be investigated as well. This is achieved by numerical simulation of small amplitude, harmonic pitching with single forcing frequency at multiples of the rotor revolution and constant Mach number (Fig. 2).
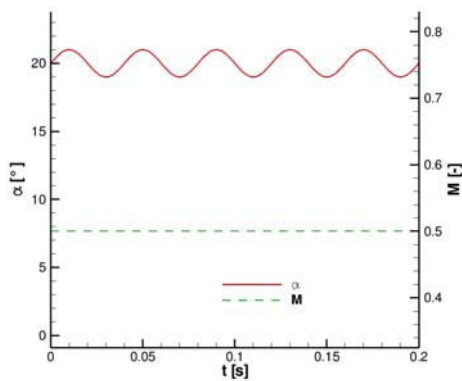
Figure 2: Angle of attack and Mach number variations for high-frequency, small amplitude pitching oscillations, **M**=0.5, α_0=20°, $\Delta\alpha$=±0.5°

Two phenomena are investigated and regarded as important characteristics of the unsteady airfoil aerodynamics. First, the damping factor is evaluated for forced sinusoidal, small amplitude pitching over a large range of mean angles of attack. The extent of negative damping thereby serves as a measure of potential pitching moment instability. Second, the amplitude between maximum and minimum resulting pitching moment coefficients is analysed at high mean angles of attack - this serves as an indication of the pitch-link loads to be expected from a torsionally oscillating airfoil on the retreating side.

These simulations in general resemble the moment stability investigations of Liiva. The Mach number and forcing frequency for the pitching airfoil were chosen as M=0.5 and f=25 Hz since these values correspond well to the rotor speed at outboard radial stations and the first torsional eigenfrequency of an economic-size helicopter.

3. NUMERICAL APPROACH

The CFD computations within the framework of the present work were performed with the DLR FLOWer code [6]. FLOWer is a block-structured, second-order, finite volume compressible (U)RANS solver applying an explicit 5-stage Runge-Kutta time integration and dual time-stepping for unsteady calculations. The ROT version of FLOWer used for the present investigations additionally allows rotational and translational rigid body movement of the grid.

3.1. URANS simulation

The extensive use of 2D URANS computations during an airfoil design process is a new approach. It enables the airfoil designer to compare different geometry variants with respect to their unsteady behavior at justifiable computational cost.

The 2D block-structured C-type meshes are script-generated. The standard grid consists of 512x128 cells with an additional block aft of the blunt trailing edge of 96x24 cells - totalling 67840 cells, the far-field boundary is situated at 50 chords distance (Fig. 3). Fine discretization has been applied to the dynamic stall and wake region for capturing of the vortex dynamics. In order to guarantee sufficient resolution of the viscous sublayer, the first wall-normal distance y^+ is calculated beforehand dependent on chord Reynolds number - fractions of this value of 0.4 and 0.8 are applied at leading and trailing edge, respectively:

$$(9) \qquad dz = 5.5 \cdot y^+ \cdot Re^{-0.875}$$
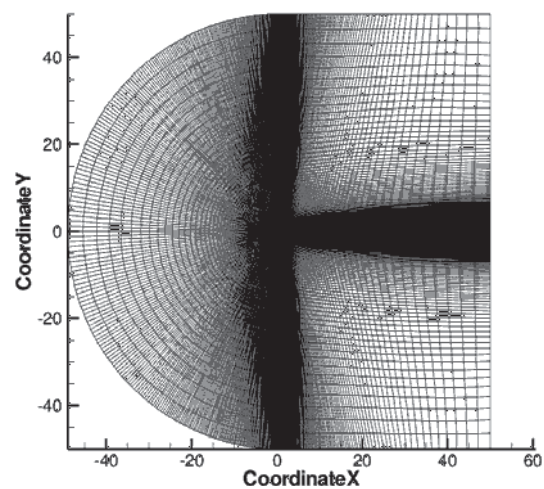
Figure 3: C-type grid topology (67840 cells) for URANS simulations of oscillating airfoils, Re-dependent spacing

The turbulence model applied to the numerical simulations is the Menter k-ω SST model, which is one of the most widely used two-equation turbulence models and applicable in case of adverse pressure gradients and flow separation. All simulations were run with fully turbulent flow such that effects of laminar-turbulent boundary layer transition are not covered by the numerical modelling.

3.2. Validation

2D URANS calculations with the block-structured DLR FLOWer code have been validated against experimental data obtained in the DNW-TWG wind tunnel [7] for the harmonically pitching OA209 rotor blade airfoil on a moderate-speed deep dynamic stall test case at M = 0.31, Re = 1.16e6, α = 9.83° ± 9.1°, and k = 0.05. A carbon-fiber model with a chord of c = 0.3m and a span of b = 1.0m was used in the 1m x 1m adaptive-wall test section of the DNW-TWG. Transition tripping was not applied. Adaptation of top and bottom walls was performed to reduce wall interferences at the position of the model. The wall shapes were adapted to the steady airfoil flow at static mean angle of attack and kept constant while the model was pitching [8]. Unsteady dynamic wall adaptation was not possible. The aerodynamic coefficients were integrated from the surface pressures measured in model center section by 45 high-speed pressure transducers. The accuracy of the pressure measurement is estimated to Δp = ±0.5% of the stagnation pressure [9]. Results were recorded for 160 periods with 128 samples per period. The measurements were affected by wind-tunnel side-wall interferences which decrease the lift measured [10]. For comparison with URANS computations, a suitable constant correction was previously found by the difference between numerically predicted lift and measured lift at static mean angle of attack. The experimental results are therefore corrected with ΔC_l = 0.0944 and ΔC_m = 0.0018.

The fully-turbulent CFD simulation, based on the measured wind tunnel airfoil geometry, was carried out with the presented grid topology and SST turbulence model. Generally, a good agreement could be achieved between experiment and numerical results with respect to the attached flow regime, i.e. for low angles of attack, Fig. 4. The deviation in lift curve slope can, to a small portion, be attributed to interferences with the far-field boundaries of the computational domain - the far-field vortex correction implemented in FLOWer is only applicable to non-moving grids. A steady computation at mean angle of attack with far-field correction resulted in a minor increase in lift on the order of 0.8%. However, wind tunnel wall effects are considered to be the main source of the observed differences. Furthermore, Menter's SST turbulence model predicts a premature trailing edge separation resulting in a loss of lift and deviation from the linear regime for angle of attacks above approximately 10°. The lift overshoot caused by the dynamic stall vortex on the airfoil's suction side can be clearly observed, even if slightly overestimated. For the fully separated flow following the dynamic stall event, the deficits of the URANS calculations become visible as the amplitude and frequency of the vortex shedding and the incidence angle for re-attachment show rather poor agreement with the experiment.
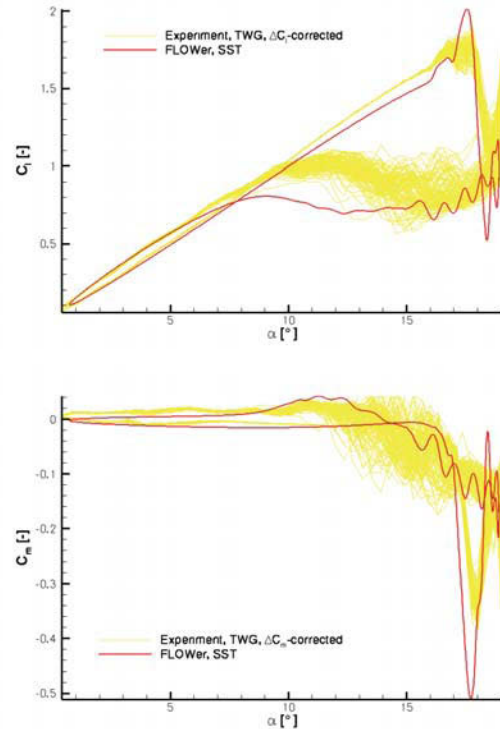
Figure 4: Validation of numerical setup with DNW-TWG experiments on the harmonically pitching OA209 airfoil, **M** = 0.31, **Re** = 1.16e6, α_0 = 9.83°, **Δα** = ±9.1°, **k** = 0.05
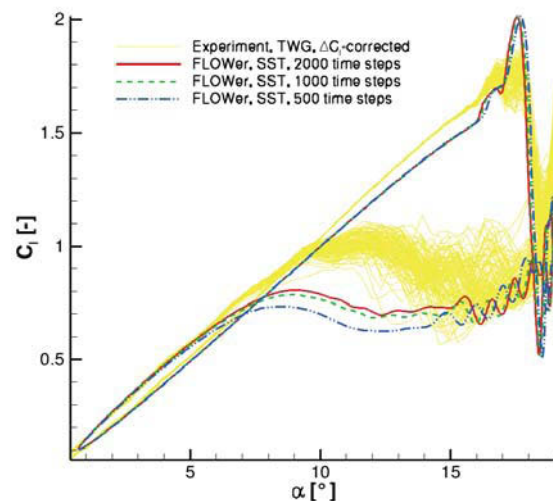
Figure 5: Influence of time resolution on the numerical simulation of the harmonically pitching OA209 airfoil, **M** = 0.31, **Re** = 1.16e6, α_0 = 9.83°, **Δα** = ±9.1°, **k** = 0.05

The accuracy of the numerical simulation is generally dependent on the chosen time resolution per cycle or time step. Especially for a pitching airfoil with separated flow and high-frequency vortex shedding over a large portion of the cycle, sufficiently small time steps are considered mandatory. In order to balance accuracy and computational cost, simulations with 500, 1000 and 2000 time steps per cycle were run. The maximum number of inner iterations remained fixed at 100. The results show

that the differences between the lift curves with 1000 and 2000 time steps are rather small and limited to the reattachment portion (Fig. 5) - unlike the very coarse time resolution of 500 time steps. A further refinement beyond 2000 time steps was therefore considered unnecessary. These findings correspond to other 2D dynamic stall validation results [11]. An additional doubling of the maximum number of 100 inner iterations during the dual time-stepping with 2000 physical time steps did not show any mentionable effect, since the density residual of $1.0 \cdot 10^{-5}$ was always reached in the attached regime, while in both cases values of up to $1.0 \cdot 10^{-3}$ were present in the fully separated part of the pitching cycle.

3.3. Rigid body movement

The cyclic pitch variations and freestream conditions of the airfoil were taken from a 3D rotor simulation by means of the comprehensive HOST flight mechanics code developed by EUROCOPTER [12], whereby the HOST blade element method aerodynamics was iteratively replaced by 3D URANS results obtained with the weakly coupled DLR code FLOWer [13]. The coupling scheme of this three-dimensional trim calculation is shown in Fig. 6.
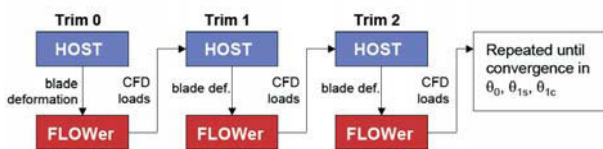
Figure 6: Coupling scheme for HOST-FLOWer trim calculations, from reference [14]

The effective angle of attack and Mach number extracted from HOST, expressed in terms of Fourier coefficients, include geometric blade twist and elastic blade torsion, superposition of flight speed, rotational velocity and downwash as well as the kinematic and elastic heaving and lagging motion.

In the 2D URANS simulations, the airfoil motion, i.e. cyclic variation of Mach number and incidence angle, was simulated by rotational and translational rigid body motion of the CFD mesh. By doing so, the phase relation between free-stream velocity and incidence angle near the blade will be exact contrary to using varying far-field boundary conditions. Only the average Mach number was prescribed as inflow condition at the far-field boundary.

4. RESULTS

4.1. Rotor environment

Mach number and angle of attack variations were extracted at radial position r/R=0.954 from a 3D trim calculation of the GOAHEAD [15] dynamic stall test case 5b. The flight condition corresponds to a fast forward flight at v=317 km/h or M=0.259 which is critical for both strong shocks on the advancing blade and dynamic stall on the retreating blade. The distributions of angle of attack and Mach number vs. azimuth angle are displayed in Fig. 1. For the 7AD rotor used in the GOAHEAD project, the

airfoil geometry at the chosen radial position corresponds to the ONERA OA209 airfoil.

Fig. 7 shows the aerodynamic coefficients of the investigated blade section, referenced by the mean dynamic pressure. This indeed resembles the variation of forces rather than coefficients due to the common denominator despite varying inflow velocity. It can be clearly observed that the first dynamic stall event - denoted by $\Delta C_{m,sh}$ in the pitching moment plot - starts at very low angle of attack of $\alpha=4.3°$. This is due to shock induced boundary layer separation in combination with increasing α as shown in the left column of Fig. 8. The shock moves upstream accompanied by an increase in thickness and streamwise extent of the separation region. The separation reduces lift and leads to both a significant drop of the pitching moment and an increase in overall drag.
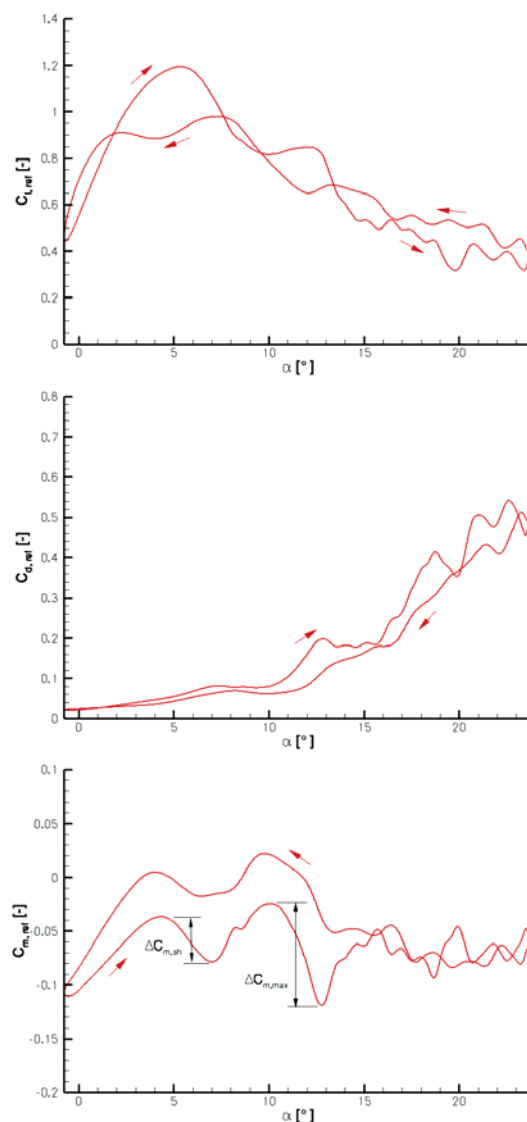
Figure 7: Aerodynamic coefficients vs. angle of attack for 2D GOAHEAD rotor-cycle simulation of r/R=0.954 blade section, test case 5b, M_{ref} = 0.5773 (mean Mach number)
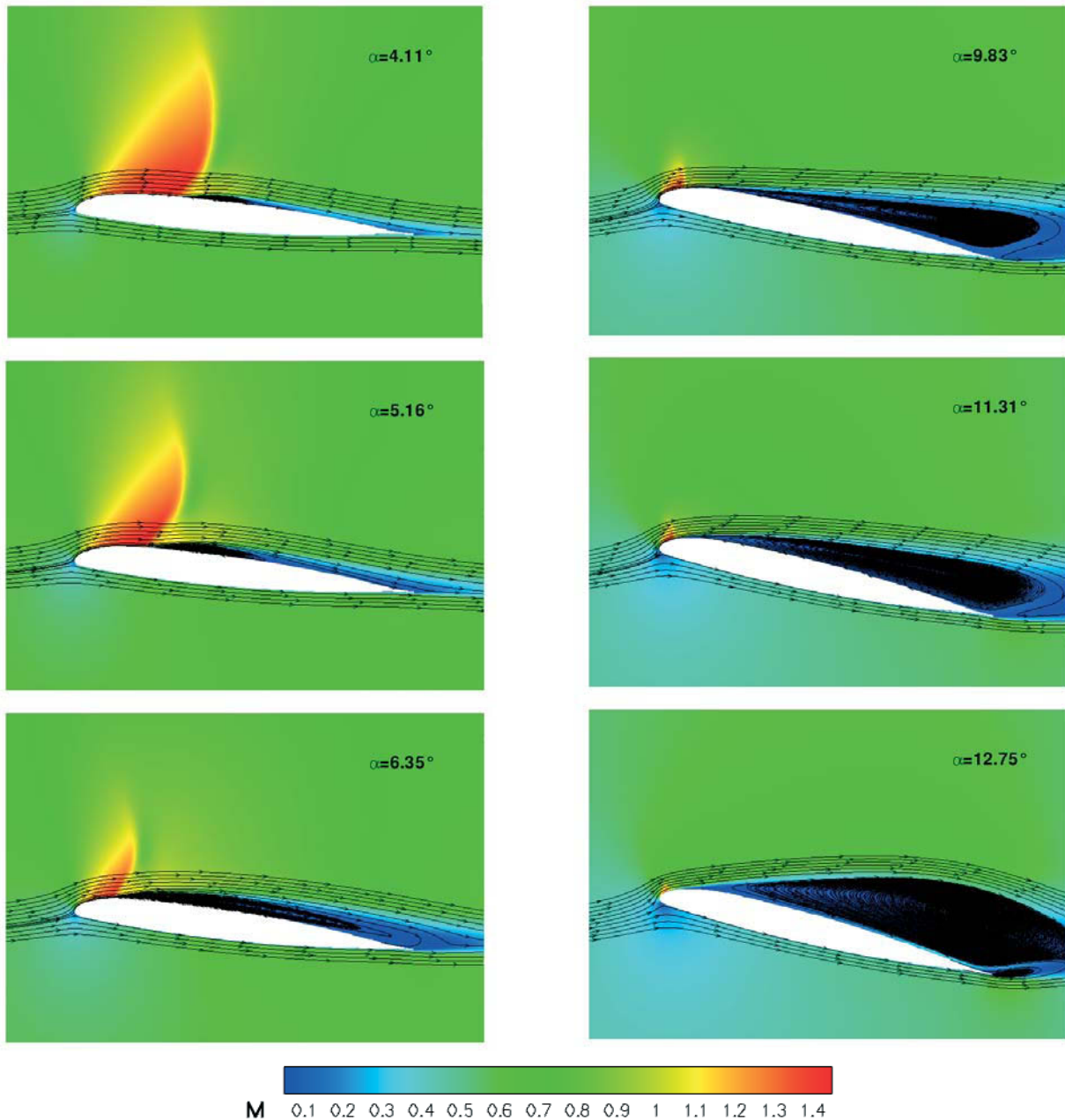
Figure 8: Mach number contour plots and streamlines for the first (left column) and second (right column) stall event for 2D GOAHEAD rotor-cycle simulation of r/R=0.954 blade section, test case 5b, M_{ref} = 0.5773 (mean Mach number)

The second stall event during the upstroke motion develops from α=10.0° onwards and is denoted by $\Delta C_{m,max}$ in the pitching moment plot of Fig. 7. It corresponds to the development and growth of a large vortex close to the trailing edge as depicted in the right column of Fig. 8, which causes a large nose-down pitching moment and an increase in pressure drag. Despite the nearly fully separated boundary layer, at the same time lift is slightly increasing due to the high induced velocities and corresponding decrease in pressure on the rear suction side of the airfoil. The remaining upstroke phase as well as the downstroke phase are dominated by the shedding of vortices - visible through oscillations in the aerodynamic coefficients in Fig. 7 - before reattachment occurs.

The unsteady assessment by means of the proposed unsteady criteria for the rotor environment is displayed in Tab. 2. The averaged loads are calculated according to formulas (1) - (3) from the CFD output of the aerodynamic coefficients. The average pitching moment coefficient has a negative sign representing a mean pitch-down moment over the rotor cycle, its magnitude is an important factor on rotor and pitch-link structural design. The aerodynamic damping S and S_i are calculated by means of a DFT of the moment coefficient's time signal and analytical solution of the ring integrals (7) and (8). It can be observed that, despite a negative value for the third higher harmonic of the rotor frequency, the overall damping is positive which correlates with the large area within a counter-clockwise C_m vs. α curve in Fig. 7. The moment

amplitudes of higher modes in the range 4-6/rev also stem from the Fourier analysis of the aerodynamic coefficients, the results of which are displayed in Fig. 9. Here, it can be seen that no dominant amplitudes lie in the frequency range under investigation. The moment peak-to-peak amplitudes are also marked in Fig. 7 and show that the original dynamic stall vortex introduces the largest dynamic loads in the URANS simulation.

Load averages	
$\overline{C_l}$	0.6714
$\overline{C_d}$	0.10044
$\overline{C_m}$	(-)0.06061
Aerodynamic damping	
S	1.176e-02
S_1	1.0566e-02
S_2	2.2809e-03
S_3	-1.2168e-03
S_4	4.2595e-05
S_5	8.7060e-05
S_6	2.2975e-06
Pitching moment higher mode amplitudes	
$|C_{m,4/rev}|$	0.002274
$|C_{m,5/rev}|$	0.002827
$|C_{m,6/rev}|$	0.001416
Pitching moment peak-to-peak amplitudes	
$\Delta C_{m,sh}$	-0.0417
$\Delta C_{m,max}$	-0.0946

Table 2: Unsteady criteria applied to the OA209 blade section in the 2D GOAHEAD rotor-cycle simulation

4.2. High-frequency oscillations

The high-frequency oscillations were simulated at a constant Mach number M=0.5 and Reynolds number Re=3.0 Mio. The pitching amplitude and frequency were set to $\Delta\alpha=\pm0.5°$ and f=25 Hz. The range of mean angles of attack was chosen between 10° and 20°. These conditions correspond to mean Mach number and torsional excitation of the first blade eigenmode for the helicopter main rotor in forward flight.
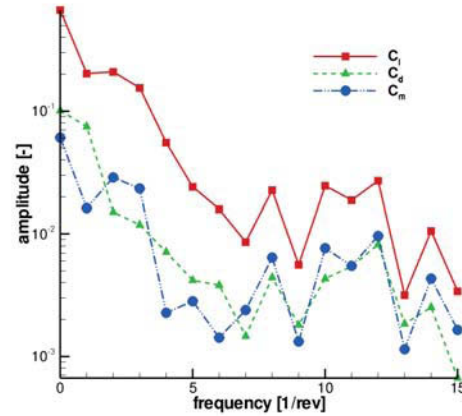
Figure 9: Amplitude spectrum for the aerodynamic coefficients for 2D GOAHEAD rotor-cycle simulation, DFT-analysis over 2 cycles

Fig. 10 shows the damping coefficient of the Liiva criterion for oscillations at different mean angles of attack. The theoretical value according to Theodorsen, Equation (6), only serves as a constant reference value for the numerical value of the moment ring integral. Since Theodorsen theory always predicts positive aerodynamic damping, the algebraic sign of the damping coefficient correctly signals damping or excitation. The main objective of this diagram is to check whether negative damping is present at certain incidence angles which would bear the risk of torsional excitation of the blade. It can be observed that, for the present flow conditions in the high subsonic range, the simulation predicts strongly negative damping for a mean angle of attack of $\alpha_{mean}=12°$ and a large variation over the range of angles of attack. Emphasis should be given to the fact that this plot is highly dependent on Mach number, such that a three-dimensional 'Liiva criterion landscape' might be an option if different flow regimes are to be investigated.

In section 2.2.2, a further criterion for dynamic loads was defined as the moment coefficient amplitudes at these high-frequency oscillations and large angle of attack. The URANS results for this criterion are shown in Fig. 11 for mean angles of attack between 16 and 20°. It can be seen that the value for a mean angle of attack of $\alpha_{mean}=20°$ is widely reduced compared to the other angles of attack. Physically, this can be attributed to streamwise shifts in the separation point along the upper surface and resulting changes in vortex magnitudes, frequencies and phases.

The differences in phase, frequency and amplitude of the pitching moment coefficient for harmonic pitching with $\alpha_{mean}=18°$ and $\alpha_{mean}=20°$ are illustrated in Fig. 12, displaying the third and fourth cycle of pitching motion. By comparison with Fig. 2, it can be further observed that the oscillations at forcing frequency are, to a different degree, phase-shifted relative to the angle of attack motion - which is of importance with regard to stability, compare Eqn. (5).
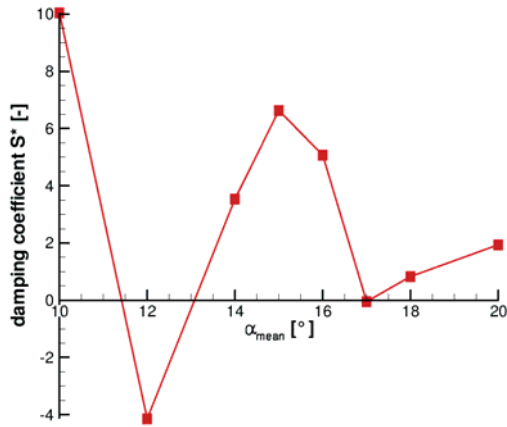
Figure 10: Amplitude spectrum for the aerodynamic coefficients for 2D GOAHEAD rotor-cycle simulation, DFT-analysis over 2 cycles
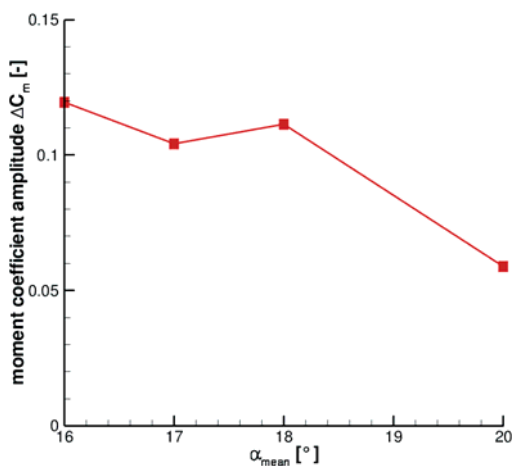
Figure 11: Maximum amplitudes of the moment coefficient oscillations for high-frequency, small amplitude harmonic pitching, M=0.5, f=25 Hz, $\Delta\alpha$=0.5°
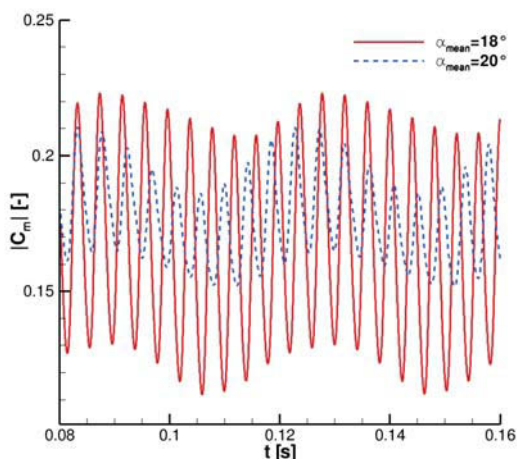
Figure 12: Absolute values of pitching moment coefficient for the third and fourth harmonic pitching cycle with α_{mean}=18° and α_{mean}=20°, M=0.5, f=25 Hz, $\Delta\alpha$=±0.5°

5. CONCLUSIONS

This paper has introduced a number of unsteady criteria for the unsteady aerodynamic assessment of airfoils based on numerical simulations. The physical reasoning for the choice of criteria has been given and one exemplary airfoil geometry has been assessed using the defined criteria. The application of the proposed criteria to different airfoil geometries is an ongoing topic of research, and first results show that characteristic differences with regard to these criteria can be established that can be considered in the airfoil design process.

The Fourier analysis to evaluate higher mode amplitudes highly depends on an accurate modelling of the vortex shedding. It is therefore planned to validate and apply different and more advanced URANS models such as RSM or models with rotational correction suitable for highly curved flows. In addition, DES computations based on the DES97 formulation and the Spalart-Allmaras turbulence model were already performed and showed a strong tendency towards grid-induced separation. The great amount of thickening of the boundary layer, due to the characteristic strong pressure gradient at the trailing edge, demands a future implementation of DDES or zonal LES and switching to a higher-order turbulence model. Finally, the influence of natural laminar-turbulent transition of the boundary layer is intended to be accounted for by appropriate transition modelling. All these efforts aim at capturing the separated flow in more detail and accuracy.

For the study of 3D effects and as a validation of the presented two-dimensional unsteady assessment criteria, supplemental 3D rotor simulations could be considered.

REFERENCES

[1]   Theodorsen, T., General Theory of Aerodynamic Instability and the Mechanism of Flutter, T.R. 496, NACA, 1935

[2]   Leishman, J. G., and Beddoes, T. S., 1989, Semi-Empirical Model for Dynamic Stall, J. Am. Helicopter Soc., 34, pp. 3.

[3]   Sheng, W., Galbraith, R. A. McD., and Coton, F. N., 2008, Modified Dynamic Stall Model for Low Mach Numbers, ASME J. Sol. Energy Eng., 130, p. 031013.

[4]   Altmikus, A., and Knutzen, B.: „Trimmed Forward Flight Simulation with CFD featuring Elastic Rotor Blades with and without Active Control", American Helicopter Society 63rd Annual Forum, Virginia Beach, VA, May 2007.

[5]   Liiva, J., Unsteady aerodynamic and stall effects on helicopter rotor blade airfoil sections, Journal of Aircraft, Vol. 6, No.1, 1969

[6]   Fassbender, J. K. and Kroll, N., editors, MEGAFLOW - Numerical Flow Simulation for Aircraft Design: Results of the Second phase of the German CFD Initiative MEGAFLOW, Vol. 89 of Notes on Numerical Fluid Mechanics and

Multidisciplinary Design (NNFM), Springer, December 2005, ISBN 9783540323822.

[7] Binder, B., Riethmüller, L., Tusche, S. and Wulf, R., Die Modernisierung des Transsonischen Windkanals in Göttingen, DGLR-Jahrestagung, Bremen, 29.09.-02.10, 1992.

[8] Geissler, W., Dietz, G., Mai, H., Bosbach, J. and Richard, H., Dynamic Stall and its Passive Control Investigations on the OA209 Airfoil Section, 31st European Rotorcraft Forum, Florence, Italy , 2005.

[9] Mai, H., Dietz, G., Geissler, W., Richter, K., Bosbach, J., Richard, H. and de Groot, K., Dynamic stall control by leading edge vortex generators, Journal of the American Helicopter Society, Vol. 53 (1), 2008.

[10] König, B., Pätzold, M. et al., Numerical and Experimental Validation of Three-Dimensional Shock Control Bumps, Journal of Aircraft, Vol. 46, No. 2, 2009, pp. 675-682

[11] Richter, K., Le Pape, A., Knopp, T., Costes, M., Gleize, V. and Gardner, A.D., Improved Two-Dimensional Dynamic Stall Prediction with Structured and Hybrid Numerical Methods, American Helicopter Society 65th Annual Forum, Grapevine (TX), USA, May 2009.

[12] Toulmay, F., Arnaud, G., Falchero, D. and Villat, V.:"Analytical Prediction of the Rotor Dynamics for Advanced Geometry Blades", American Helicopter Society, 52nd Annual Forum, Washington, D.C., June 1996.

[13] Dietz, M., "Simulation der Umströmung von Hubschrauberkonfigurationen unter Berücksichtigung von Strömungs-Struktur-Kopplung und Trimmung", Dissertation Universität Stuttgart (2009), ISBN 9783899639421

[14] Dietz, M., Kessler, M. and Krämer, E., Aeroelastic Simulations of Isolated Rotors Using Weak Fluid-Structure Coupling, High Performance Computing in Science and Engineering '06, Springer, October 2007, ISBN 9783540361657, pp. 407-420

[15] Pahlke, K., The GOAHEAD Project, 33rd European Rotorcraft Forum, Kazan, Russia, September 2007